Journal of The Electrochemical Society, **152** (4) A837-A844 (2005)
0013-4651/2005/152(4)/A837/8/$7.00 © The Electrochemical Society, Inc.

In Situ Determination of MEA Resistance and Electrode Diffusivity of a Fuel Cell

Jürgen Stumper,[a,*,z] Herwig Haas,[a] and Ana Granados[b]

[a]*Ballard Power Systems, Incorporated, Burnaby, British Columbia V5J 5J9, Canada*
[b]*Pacific Institute for Mathematical Sciences, University of British Columbia, Vancouver, British Columbia V6T 1Z2, Canada*

This paper describes a novel method to determine the membrane electrode assembly (MEA) resistance and electrode diffusion (MRED) coefficient for a fuel cell (the MRED method) under *in situ* conditions. It is shown that the MRED method allows the determination of (*i*) the ohmic resistance of an MEA and (*ii*) the mass-transport coefficient of the electrodes. The method is based on the galvanostatic discharge of a fuel cell with interrupted reactant supply. Application of the method to the cathode of a polymer electrolyte membrane fuel cell is demonstrated, and the experimental results are analyzed using a theoretical model based on a simple one-dimensional diffusion process using Fick's law. Comparison of the experimental O_2 mass-transport coefficient with theoretical values indicates that diffusion in the active layer is mass-transport limiting.
 [DOI: 10.1149/1.1867673]

Manuscript submitted September 2, 2004; revised manuscript received October 5, 2004. Available electronically March 15, 2005.

To meet the power density, reliability, and cost requirements that enable a widespread use of fuel cells, cost reduction and increased power output remain key challenges. To reduce development time and cost, a rapid and convenient means for the optimization of fuel cell designs is needed. This requires foremost a sufficient understanding of the structure-property-performance relationships for the fuel cell and its components. In particular, the dependence of cell voltage and cell voltage degradation on the physicochemical and structural properties of the components of the fuel cell must be better understood. Due to the complexity of the heat- and mass-transport processes occurring in fuel cells, there is typically a multitude of parameters to be determined. Therefore, the challenge is the identification of those critical parameters that which have the highest impact on fuel cell performance. This can be done through either theoretical or empirical models, which can then be used as design tools to optimize fuel cell designs more quickly. For the development of these design tools, accurate measurement tools are needed to provide reliable data to establish empirical correlations, to provide model inputs, or to validate model predictions.

In this study, we present a novel method for determination of the cell resistance and the effective diffusion coefficient for a fuel cell cathode, which can be used as a measurement tool to provide valuable experimental data for the investigation of the structure-performance relationships for fuel cell electrodes. The membrane electrode assembly (MEA) resistance and electrode diffusion (MRED) method allows the investigation of the effect of operating conditions as well as structural properties of the electrodes on performance and can thus support the development of improved design tools for fuel cells.

Generally, the cell voltage losses can be kinetic, ohmic, and mass-transport related;[1] therefore, one of the design challenges is to optimize electrode structures so that these cell voltage losses are minimized. Especially on the oxidant side mass-transport losses associated with transport of reactants and products to and from the active catalyst sites are a major cause for performance inefficiencies of fuel cells. The most widely used method for the determination of the different voltage loss components for the cathodic reaction consists of the least-squares fitting of an analytical expression comprising all the various loss components to the experimental cell voltage *vs.* current density (*E vs. i*) curves. Srinivasan and co-workers[2] have been using the simple equation

$$E = E^0_{\text{cell}} - b \cdot \log\left(\frac{i}{i_0}\right) - iRA \qquad [1]$$

to fit experimental *E vs. i* curves. Here, E^0_{cell}, i_0, b, R, and A denote the reversible cell voltage, exchange current density, Tafel slope, cell resistance, and cell area, respectively. The typical assumption here is that the anodic contribution to the total overpotential is small compared to the cathodic contribution, which is generally justified for pure H_2 operation. However, Eq. 1 contains no explicit term for the mass-transport or diffusion overpotential and therefore does not account for deviations from the linear behavior observed at higher current densities and/or lower oxygen concentrations on the cathode. Also, the resistance R as determined from a fit of Eq. 1 to experimental data should more appropriately be labeled pseudo-ohmic[3] as it depends on operating conditions such as current density and gas composition and is therefore partially determined by mass-transport effects as well. Rho and co-workers compared polymer electrolyte membrane (PEM) fuel cell performances for helox (O_2/He), O_2/Ar, and O_2/N_2 mixtures as cathodic reactants and showed that R depends on the inert component and, more strongly, on the cathode gas pressure.[4] To more accurately describe the *E vs. i* behavior including mass-transport effects, Kim *et al.* extended Eq. 1 by including an empirical term[5] $m \cdot \exp(ni)$

$$E = E^0_{\text{cell}} - b \cdot \log\left(\frac{i}{i_0}\right) - iRA - m \cdot \exp\left(n\frac{i}{i_0}\right) \qquad [2]$$

The disadvantage of this approach is that it does not provide a physicochemical interpretation of the associated fit parameters m,n. Another alternative is the inclusion of a mass-transport related concentration overpotential η_c based on Fick's law of diffusion[6]

$$E = E^0_{\text{cell}} - b \cdot \log\left(\frac{i}{i_0}\right) - iRA - \eta_c \qquad [3]$$

where

$$\eta_c = \frac{\Re T}{nF} \ln\left(\frac{i_{\max}}{i_{\max} - i}\right) \qquad [4]$$

However, upon fitting experimental data with an equation based on Eq. 3, this approach suffers from an interdependence of R and the mass-transport related limiting current $i_{\max}$. However, Squadrito *et al.*[7] have described the mass-transport loss η_c by a term such as the one in Eq. 4 multiplied by an amplification term $\alpha(i/i_0)^k$

$$\eta_c = \alpha\left(\frac{i}{i_0}\right)^k \cdot \frac{\Re T}{zF} \ln\left(\frac{i_{\max}}{i_{\max} - i}\right) \qquad [5]$$

The amplification term takes into account nonlinear effects arising from mutual correlations between the mass-transport contributions of different MEA components such as diffusion and catalyst layers as well as the fact that the local operating conditions depend on the (x,y) position within the MEA area. However, as with the empirical

* Electrochemical Society Active Member.
z E-mail: jurgen.stumper@ballard.com

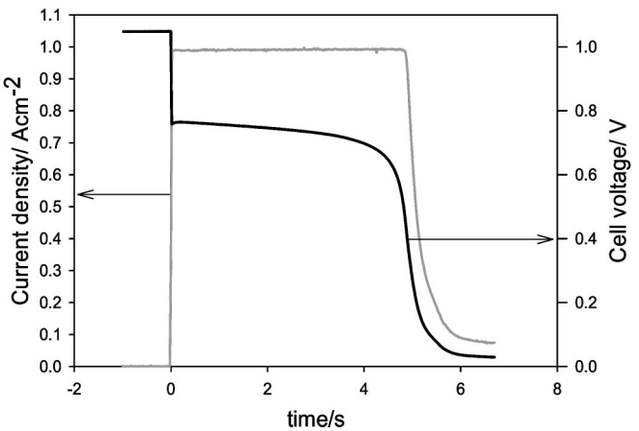

Figure 1. Cell voltage transient under H_2/O_2 operation at $i = 1$ A/cm^2. Operating conditions: H_2/O_2, $T = 75°C$, $p = 300$ kPa, fuel inlet open, O_2 valves closed.

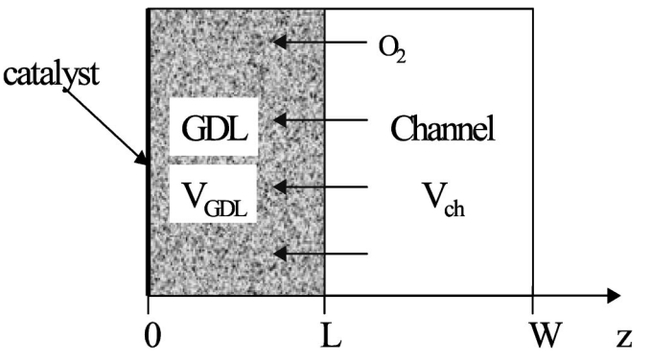

Figure 2. Schematic diagram for cross section of an electrode. L: electrode thickness, $W = V_{tot}/A$ where $V_{tot} = V_{GDL} + V_{ch}$ is the total cathode volume, A: cell active area.

term added by Kim *et al.*, the fit parameters α,k do not allow a quantitative determination of mass-transport related fuel cell properties.

Hence, in this study we present a novel method that allows the separation of the ohmic and mass-transport related performance losses of a fuel cell and yields (i) the true ohmic cell resistance unaffected by mass-transport effects and (ii) the effective O_2 diffusivity of the cathode electrode including the catalyst layer.

Theoretical Analysis of Cell Voltage Transients during Cathode Discharge

During a cathode discharge experiment according to the MRED method, the cathode compartment is separated from the gas supply by closing both inlet and outlet valves, whereas the anode side continues to be supplied with H_2. Then the load is switched on (i = const.), and the cell voltage transient is recorded during the discharge of the fuel cell. The resulting discharge curve (see Fig. 1) is similar to those observed on batteries. The initial voltage drop after the current has been switched on ($t = 0$) is due to the ohmic and kinetic overpotentials, which react practically instantaneously (on a time scale larger than the charging of the double layer). However, no mass-transport losses are present at $t = 0$ as the O_2 concentration at the catalyst sites is identical to the bulk concentration in the flow channels. However, the rapidly accelerating voltage decrease observed for times $t > 0$ is determined by (i) the decrease in O_2 concentration in the cathode compartment and (ii) the O_2 concentration gradient across the electrode necessary to sustain the external current.

In the following sections, we (i) develop a solution for the O_2 concentration $c(0,t)$ at the catalyst sites by solving the corresponding differential equation with the appropriate boundary conditions and (ii) show how the O_2 concentration $c(0,t)$ at the catalyst sites can be calculated by using the measured $E_{cell}(t)$ profiles. Using the MRED method it is possible to extract valuable information on the mass-transport properties of the electrode *in situ* under fuel cell operating conditions.

Calculation of O_2 concentration during cathodic discharge.—We use the schematic diagram in Fig. 2 for the discussion of the discharge experiment. We describe the electrode as a single layer of thickness L with the catalyst located at $z = 0$.

To model the transport of O_2 through the gas diffusion layer (GDL) we assume the following.

1. The electrode is modeled as a single layer with a catalyst layer of zero thickness.
2. A one-dimensional (1D) model is used for the GDL using Fick's law.
3. No production/condensation of water vapor and associated convective effects are considered.
4. The effect of liquid water in the GDL on O_2 diffusion is ignored.
5. Heat transfer effects are neglected.
6. The current density i is constant during discharge.

Even though most fuel cells operate with air instead of oxygen on the cathode, we compare our model predictions with experimental data obtained for pure O_2. The intent is to include O_2/inert gas mixtures in the future.

We denote by $c(z,t)$ the O_2 concentration in the GDL and by $c_{ch}(t)$ the O_2 concentration in the flow field channels. The differential equation for $c(z,t)$ is then

$$\frac{\partial}{\partial t}c(z,t) = D_{eff}\frac{\partial^2}{\partial z^2}c(z,t) \qquad [6]$$

where D_{eff} is the effective O_2 diffusion coefficient of the cathode electrode. The boundary conditions are as follows

$$c(z,0) = c_0$$

$$4FD_{eff}\frac{\partial}{\partial z}c(0,t) = i \quad \text{for } t > 0 \qquad [7]$$

where F is Faraday's constant. The boundary condition at the GDL/channel interface can be written as

$$c(L,t) = c_{ch}(t) \qquad [8]$$

where $c_{ch}(t)$ satifies the following partial differential equation

$$\frac{\partial}{\partial t}c_{ch}(t) = -\frac{AD_{eff}}{V_{ch}} \cdot \frac{\partial}{\partial z}c(z,t)\bigg|_{z=L} \qquad [9]$$

with the initial condition

$$c_{ch}(0) = c_0 \qquad [10]$$

A theoretical solution (see the Appendix) of Eq. 6-10 is shown in Fig. 3, where $c(0,t)$ and $c_{ch}(t)$ are displayed for a range of diffusion coefficients and $i = 1$ A/cm^2. See also Fig. 4.

After a short initial relaxation time on the order of $t_r \approx L^2/D_{eff}$, the O_2 concentration at the catalyst sites decreases at the same rate as the O_2 concentration in the channel. We also note that the concentration difference $\Delta c = c_{ch}(t) - c(0,t)$ is time independent and a function of D_{eff} only. Under these quasi-stationary conditions, Eq. 7 yields

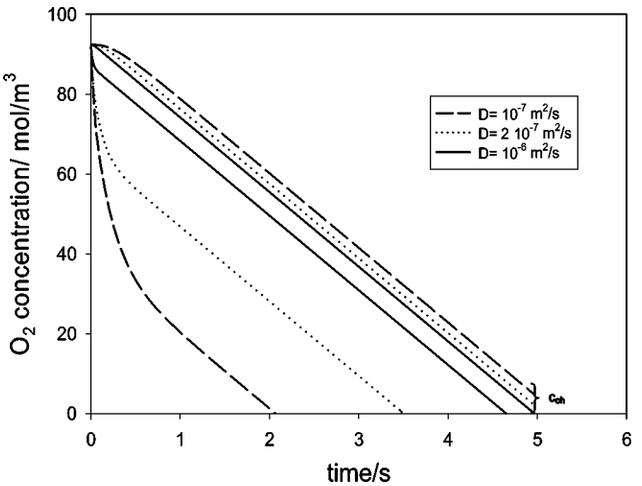

Figure 3. Analytical solution for time dependence of $c_{ch}(t)$ (upper three curves) and $c(0,t)$ (lower three curves) for current density of $i = 1$ A/cm^2, $V_{ch} = 34.6$ cm^3, $V_{tot} = 42.1$ cm^3, $c_0 = 92.3$ mol/m^3, $L = 250$ μm, and a range of diffusion coefficients $D_{eff} = 10^{-7}$ m^2/s, $D_{eff} = 2 \times 10^{-7}$ m^2/s, and $D_{eff} = 10^{-6}$ m^2/s.

$$\Delta c = c_{ch}(t) - c(0,t) = \frac{iL}{4FD_{eff}} \qquad [11]$$

Therefore, if Δc can be derived from experimental data, then Eq. 7 allows the determination of the effective O_2 diffusion coefficient D_{eff} of the electrode. Whereas $c_{ch}(t)$ can be measured simply using a pressure sensor, the calculation of $c(0,t)$ from the cell voltage transient during discharge is explained in the next section.

Calculation of oxygen concentration c(0,t) at catalyst layer from cell voltage transient $E_{cell}(t)$.—The cell voltage can be expressed as

$$E_{cell}(t) = E^0_{cell}(t) - \eta_c(t) - \eta_a - iRA \qquad [12]$$

where E^0_{cell} is the reversible cell voltage, η the overpotential, and the subscripts a,c denote the anode and cathode, respectively. In Eq. 12 we further assume that the overpotential for the anode is constant after the current has been switched on at $t = 0$ as H_2 is continuously being supplied during the discharge, *i.e.*, the cell voltage decrease is interpreted exclusively as the change in the reversible cell voltage $E^0_{cell}(t)$ and the overpotential $\eta_c(t)$ on the cathode side.

The cell voltage decay can therefore be expressed as

$$E_{cell}(0) - E_{cell}(t) = E^0_{cell}(0) - \eta_c(0) - E^0_{cell}(t) + \eta_c(t) \qquad [13]$$

The time dependence of the reversible cell voltage can be calculated using the Nernst equation for the cathode

$$E^0_c(t) = E^0_{c,ref} + \frac{\Re T}{2F} \ln\left(\sqrt{\frac{c_{ch}(t)}{c^{ref}}} \cdot \left(\frac{c_{H^+}}{c_{H^+}{}^{ref}} \right)^2 \cdot \frac{c_{H_2O}{}^{ref}}{c_{H_2O}} \right) \qquad [14]$$

where $E^0_c(t)$ is the reversible cathode potential. $E^0_c(t)$ is time dependent as the O_2 concentration in the flow channels $c_{ch}(t)$ continually decreases during the discharge. Assuming c_{H^+}, c_{H_2O} are time independent, it follows that

$$E^0_{cell}(0) - E^0_{cell}(t) = \frac{\Re T}{2F} \ln\left(\sqrt{\frac{c_{ch}(0)}{c_{ch}(t)}} \right) \qquad [15]$$

$\eta_c(t)$ can be expressed as a function of the oxygen concentration at the catalyst layer using the Tafel equation

$$i(t) = i^0_c \cdot \frac{c(0,t)}{c_{ref}} \cdot \exp\left(2.303 \frac{\eta_c(t)}{b_c} \right) \qquad [16]$$

where i^0_c denotes the exchange current density, $c(0,t)$ the oxygen concentration at the catalyst layer, c_{ref} a reference concentration (*e.g.*, $p_{O2} = 1$ atm), and b_c the Tafel slope, which leads to

$$\eta_c(t) - \eta_c(0) = b_c \cdot \log\left(\frac{c(0,0)}{c(0,t)} \right) \qquad [17]$$

With Eq. 15 and 17, Eq. 13 simplifies to

$$E_{cell}(0) - E_{cell}(t) = b_c \cdot \log\left(\frac{c(0,0)}{c(0,t)} \right) + \frac{\Re T}{2F} \ln\left(\sqrt{\frac{c_{ch}(0)}{c_{ch}(t)}} \right) \qquad [18]$$

Equation 18 does not contain any ohmic contribution as the ohmic overpotential remains constant during the transient. Thus, the change in cell voltage over time is due to the change of the ratio $c(0,0)/c(0,t)$ at the catalyst sites corrected with respect to the change in oxygen concentration in the flow field channels which act as a reactant reservoir. Therefore, the cell voltage transient during cathode discharge can be considered as an electrotitration of O_2 at the cathode catalyst sites.[8]

With Eq. 18 we can now calculate the O_2 concentration $c(0,t)$ at the catalyst sites as a function of time using the fact that without current ($t = 0$) the O_2 concentration at the catalyst sites equals the O_2 concentration in the flow channels. With

$$c(0,0) = c_{ch}(0) = c_0 \qquad [19]$$

it follows that

$$c(0,t) = c_0 \cdot \exp\left(-2.303 \frac{E_{cell}(0) - E_{cell}(t) - \frac{\Re T}{2F} \ln\left(\sqrt{\frac{c_0}{c_{ch}(t)}} \right)}{b_c} \right) \qquad [20]$$

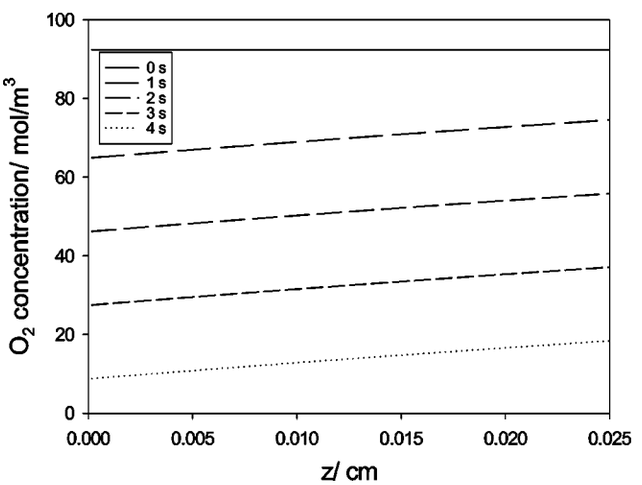

Figure 4. Calculated profile (see Appendix) of O_2 concentration across the GDL for different times; $i = 1$ A/cm^2, $D_{eff} = 6.1 \times 10^{-7}$ m^2/s, other parameters as in Fig. 3.

Experimental

The experimental results were obtained using a single Ballard Mk 9 MEA with a Nafion 112 membrane. The data acquisition system consisted of a PXI-1002 chassis with an embedded processor coupled to an SCXI-1001 chassis via a PXI-6052E 16 bit data acquistion card from National Instruments Corporation connected to a personal computer.

The test cell was operated on a custom-designed test station allowing accurate control and monitoring of all operating parameters.

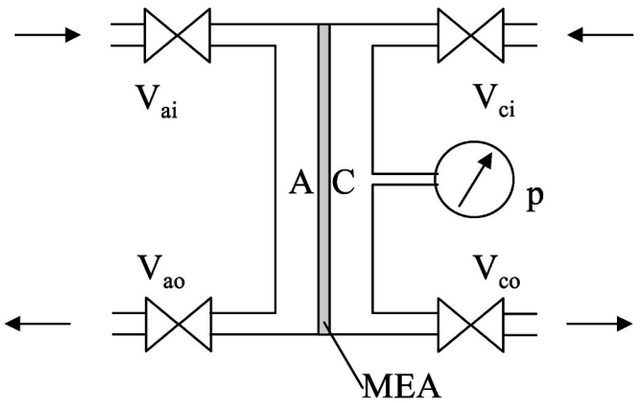

Figure 5. Schematic diagram of experimental setup. p: pressure sensor, V_{ai}, V_{ao}, V_{ci}, V_{co} are anode and cathode inlet and outlet valves, respectively. A: anode, C: cathode.

Steady-state polarization curves were obtained under constant fuel and oxidant stoichiometry with respect to the total cell current. For a transient polarization, the cathode inlet and both outlet valves (see Fig. 5) were closed. The anode inlet valve was left open to keep the H_2 pressure constant during discharge. After each discharge, the cathode inlet and outlet valves were opened for ≈1 s to recharge the cell for the next transient experiment. Cell temperatures are given by the coolant inlet temperature.

Results and Discussion

Figure 1 shows a typical cell voltage transient for H_2/O_2 operation at $i = 1$ A/cm^2 together with the load current. At $t = 0$ the current is switched on and the the cell voltage drops to its initial value $E_{cell}(0)$. The current stays constant until $E_{cell}(t)$ drops to about 0.4 V, a cutoff point that is determined by the characteristics of the electronic load used for the experiment. Figure 6 shows a series of cell discharge voltage profiles obtained at a range of different current densities. When displayed against charge instead of time, all transients correspond to the same charge capacity Q

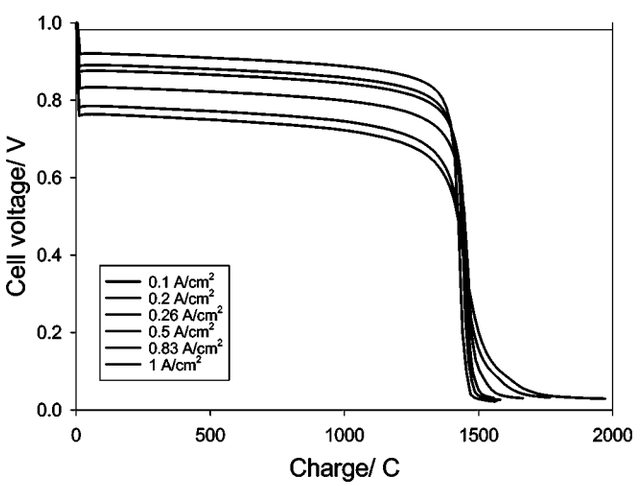

Figure 6. Cell voltage transients for various current densities for closed cathode compartment *vs.* capacity. Operating conditions: H_2/O_2, $T = 75$°C, $p = 300$ kPa, fuel inlet open. Topmost curve of the graph corresponds to the lowest current density.

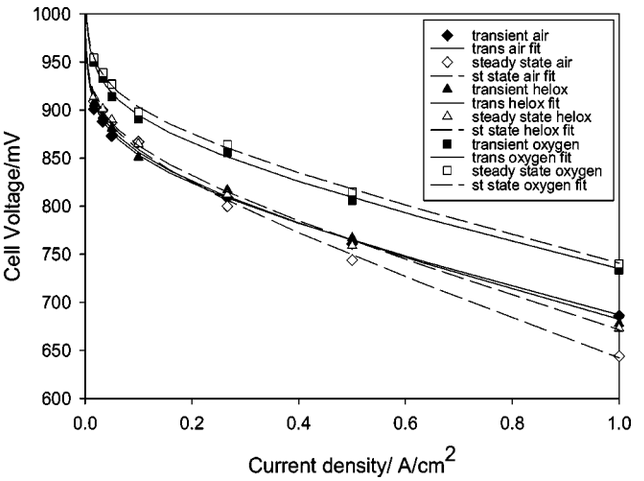

Figure 7. Comparison between transient and steady-state polarization; transient voltages $E_{cell}(0,i)$ were taken at charge $Q = 6$ C. Symbols: experimental data, lines: fit of Eq. 1. Squares: oxidant O_2, triangles: oxidant helox, diamonds: oxidant air, full symbols: transient polarization, open symbols: steady-state polarization, other operating conditions: fuel = H_2, $T = 70$°C, $p = 300$ kPa. (i) Transient polarization: anode inlet open, cathode inlet and outlet valves closed. (ii) Steady-state polarization, H_2 stoich 1.5; O_2, helox, air stoich: 10, 2, 2.

$$Q \approx c_0 4FV_{tot} \qquad [21]$$

of about 1500 C(=0.41 Ah). With Eq. 21 the total cathode free volume V_{tot} can be estimated to be about 38.8 cm^3, which is large compared to the amount of product water per discharge of about 0.135 cm^3. This justifies the assumption of V_{tot} = const. during the discharge experiment.

From the discharge transients in Fig. 6, the initial or "transient" cell voltage $E_{cell}(0)$ can be extracted and plotted against current density i (transient polarization curve). Figure 7 shows transient polarization curves for three oxidant gases: O_2, helox, and air. The corresponding traditional steady-state polarization curves are also shown for comparison. For air, the transient polarization curve lies markedly above the steady-state polarization, whereas for helox, the difference is reduced to less than ≈15 mV. For O_2, the two polarizations are practically identical. This indicates the presence of increased mass-transport losses under steady-state operation when changing reactants from O_2 over helox to air. The results of a fit of Eq. 1 to the experimental data shown in Table I confirm this, showing a monotonic increase in the steady state "pseudo" resistance from O_2 to air. However, the transient resistances R_t are essentially the same within the error (average $R_t = 120$ mΩ cm^2) and in agreement with the O_2 steady-state resistance, further supporting the fact that R_t measures the actual ohmic fuel cell resistance independent of the reactants.

Figure 8 shows an experimental result together with a model calculation for the time dependence of the O_2 concentrations in the flow channels and at the catalyst sites calculated using Eq. 20. The O_2 concentrations in the flow channels and at the catalyst sites decrease linearly with time as long as the current i is constant except at short times (<0.5 s), where relaxation effects[9] play a dominant role. The observed time independence of $\Delta c(t)$ shows that a simple 1D Fickian diffusion model with a time-independent O_2 diffusion coefficient provides a satisfactory explanation of the observed voltage transients during cathode discharge. Moreover, this also implies that the thus determined effective O_2 diffusion coefficient D_{eff} is pressure independent. The total cathode volume $V_{tot} = 42.1$ cm^3 used for the model calculations is slightly larger than the value determined from Eq. 21, the difference indicating that there probably remains some residual O_2 after completion of the transient.

Table I. Results of least-squares fit of Eq. 1 to transient and steady-state polarization curves in Fig. 7. Errors for the fit parameters correspond to a doubling of the χ_2 error (while all other fit parameters are held constant), ε is the mean relative error of the fit.

	E_0 (mV)	b (mV)	R/mΩ cm^2	Fit error, ε (%) $\varepsilon = \sqrt{\frac{1}{n}\sum_{j=1}^{n}\left(\frac{y_j^{data}-y_j^{fit}}{y_j^{data}}\right)^2}$
O_2 transient	848 ± 5	58 ± 3	113 ± 7	0.36
O_2 steady state	862 ± 3	53 ± 3	121 ± 6	0.31
Helox transient	811 ± 4	58 ± 3	128 ± 10	0.53
Helox steady state	825 ± 3	53 ± 3	153 ± 7	0.38
Air transient	807 ± 6	58 ± 5	120 ± 14	0.72
Air steady state	824 ± 5	53 ± 5	181 ± 12	0.63

For the experimental determination of D_{eff} according to Eq. 11 the discharge experiment is repeated for different currents and the resulting Δc plotted against i. Figure 9 shows that Δc is proportional to the current density. As $c(0,t)$ is very sensitive to the value of $E_{cell}(0)$, the transient cell voltage after switching on the current, a nonlinear fit routine was used to extract those values for $E_{cell}(0)$ that minimized the error between the calculated $c(0,t)$ and a straight line parallel to $c_{ch}(t)$. In all cases, the fitted $E_{cell}(0)$ was within ±5 mV of the experimental value.

The experimental value for the mass-transfer coefficient $D_{eff}/L = 2.44 \times 10^{-3}$ m/s determined from the linear fit is close to the value of $D_{eff}/L = 2.8 \times 10^{-3}$ m/s that was determined independently using a nonlinear four-parameter fit to experimental helox and air polarization curves obtained with a similar setup and fuel cell.[10] Using $L = 2.5 \times 10^{-4}$ m, these experimental values correspond to $D_{eff} = 6.1 \times 10^{-7}$ m^2/s and $D_{eff} = 7.2 \times 10^{-7}$ m^2/s, respectively, which are more than an order of magnitude smaller than the binary diffusion coefficients D_{ij} for O_2 in H_2O vapor, N_2, or He (see Table II). This difference could be due to (i) local 2D effects related to the flow channel geometry, (ii) the presence of liquid water in the GDL reducing the porosity, or (iii) the presence of a secondary layer limiting the O_2 diffusivity of the electrode.

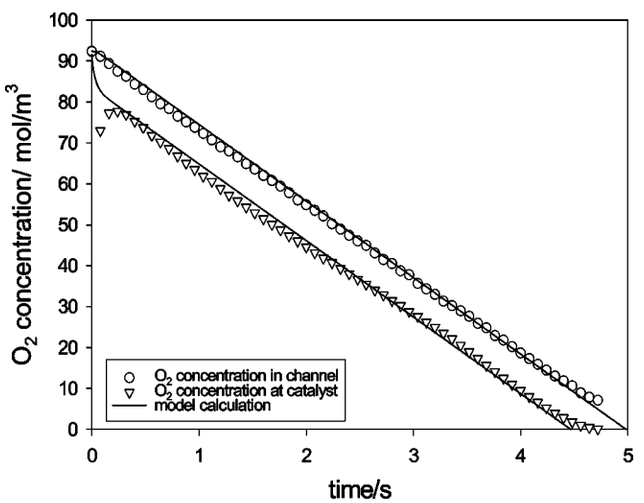

Figure 8. Experimental and theoretical time dependence of oxygen concentrations in flow field channels c_{ch} and at catalyst layer $c(0,t)$ for the experiment in Fig 1. Symbols: experimental data, lines: model calculation. Operating conditions: H_2/O_2, p = 300 kPa, T = 75°C, i = 1 A/cm^2, O_2 inlet and outlet valves closed, H_2 inlet valve open, H_2 outlet valve closed. O_2 concentration c_{ch} was corrected for water vapor concentration assuming RH = 100%. $C(0,t)$ (triangles) was calculated from cell voltage transient in Fig. 1. Theoretical calculations were performed as outlined in the Appendix with $D_{eff} = 6.1 \times 10^{-7}$ m^2/s, $V_{ch} = 34.6$ cm^3, $V_{tot} = 42.1$ cm^3, $c_0 = 92.3$ mol/m^3.

Case (i).—Local 2D effects could be caused by the fact that reactants must deviate from the through plane (z) direction to reach catalyst sites located under the flow channel landings. Although this would increase the diffusion length, an increase of no more than 50% can be expected for the plate geometry used in the experiments.

Case (ii).—The presence of a porous medium generally inhibits gas diffusion, which can be taken into consideration using a Bruggeman-type correction[11]

$$D_{eff} = \varepsilon^{1.5} D_{O_2} \quad [22]$$

under the assumption of a hard sphere model for the porous structure. ε denotes the porosity of the porous material and D_{O_2} the free space O_2 diffusion coefficient. From Eq. 22 it follows that a diffusivity reduction by a factor of 10 would mean a porosity of $\varepsilon \approx 0.21$, compared to a value of 0.7-0.8 for the porosity of a dry GDL. To explain the low experimental value for D_{eff} (more than one order of magnitude difference), we therefore have to assume a liquid water saturation of >75% for the GDL, which seems rather high. In a recent study,[12] it was reported that liquid water saturation levels of the GDL even at 1.4 A/cm^2 do not exceed 10%.

Case (iii).—The fact that the mass-transfer coefficient is essentially independent of the gas composition could also indicate that another transport process such as diffusion through the active (catalyst) layer (in series with diffusion though the GDL) determines the O_2 flux to the catalyst sites. Typically, electrodes are fabricated us-

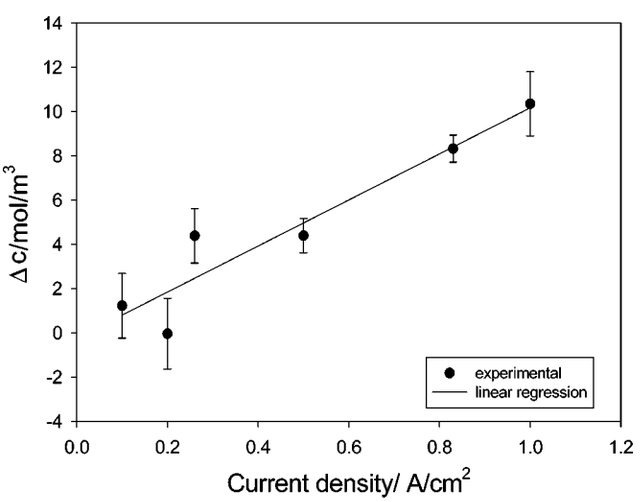

Figure 9. Experimental plot of Δc *vs.* current density i. Circles: experimental values, solid line: straight line least-squares fit, other parameters: b_c = 55 mV, T = 75°C, L = 250 μm. Error bars represent experimental errors in voltage and pressure measurements. Experimental value for effective O_2 diffusion coefficient: $D_{eff} = 6.1 \times 10^{-7}$ m^2/s.

Table II. Binary diffusion coefficients for gas mixtures calculated using the Fuller, Schettler, Giddings relationship[15] for p = 300 kPa, T = 70°C.

Gas mixture	Binary diffusion coefficients, D_{ij} (10^{-5} m^2/s)
O_2-N_2	0.883
O_2-He	3.06
O_2-H_2O	1.12

ing a highly porous substrate such as carbon fiber paper which is coated with one or more (active) layers containing carbon black, poly(tetrafluoroethylene), a proton conductor (Nafion), and catalyst particles.[13]

Using the O_2 diffusion coefficents in the membrane or the active layer reported in the literature (see Table III) and the experimental value for D_{eff}/L, the diffusion length L_{exp} in the active layer can be estimated. Table III shows that L_{exp} ranges from 0.02 to 8 μm. This appears reasonable considering the physical thickness of the active layer (typically in the order of several 10 μm), which should constitute the upper boundary for the diffusion length. Consequently, the assumption of a transport-limiting step in the active layer seems the most plausible explanation for the low value for D_{eff}.

The bilayer model for the electrode also explains the observed independence of D_{eff} on pressure. In the substrate layer, O_2 transport is governed by continuum diffusion (and/or viscous flow), where molecule-molecule collisions dominate over molecule-wall conditions. Continuum diffusion is described by the binary diffusion coefficients D_{ij} (see Table II), which are inversely proportional to the total gas pressure. According to Eq. 11, this would lead to a pressure (time) dependence of Δc contrary to the experimental observations.

The mean free path length for O_2 at 300 kPa and 70°C is about 5.5 nm, which is on the same order of magnitude as the particle size in the active layer. Therefore, O_2 transport through the active layer most likely is dominated by interactions with the pore walls (Knudsen diffusion). The corresponding Knudsen flow parameters D_{iK} are independent of the total gas pressure[20] leading to a time-independent Δc in agreement with the experimental results.

Conclusions

A novel *in situ* method has been developed to determine the MRED of a fuel cell electrode under operating conditions. The MRED method (i) provides, information on both the kinetic and resistive cell parameters without interference by mass-transport effects (by means of the transient polarization) and (ii) additionally allows the determination of the effective reactant diffusion coefficient D_{eff} of the electrodes.

The MRED method was applied to the cathode electrode of a PEM fuel cell to determine the pure ohmic resistance of the MEA and the effective diffusion coefficient D_{eff} for O_2 for the cathode electrode. A comparison of the results for pure O_2, air, and O_2/He mixtures showed that D_{eff} is (i) essentially independent of reactant gas composition and (ii) independent of the total gas pressure. This indicates that the active layer in the electrodes, where Knudsen diffusion dominates due to the small pore size, is most probably mass-transport limiting. The calculated diffusion length in the active layer covers a relatively wide range from 0.02 to 8 μm due the large spread in literature values for the active layer O_2 diffusion coefficient.

An analytical solution was developed for the cathode discharge of a fuel cell using an iterative procedure. Assuming a simple 1D Fickian diffusion process with time-independent diffusion coefficient, good agreement was found between model and experiment.

Although the experimental results reported in this study only apply to the cathode of a PEM fuel cell, the MRED method can also be used on the anode side to provide information on the H_2 diffusion properties of the anode. Furthermore, the method appears to be applicable to any type of fuel cell that can tolerate a pressure differential across the gas separator.

Table III. O_2 diffusion coefficients for Nafion membranes and active layer reported in the literature together with diffusion lengths L_{exp} calculated using experimental result for D_{eff}/L.

	Membrane		Active layer	
Reference	D_{O2} (10^{-8} m^2/s)	L_{exp} (μm)	D_{O2} (10^{-8} m^2/s)	L_{exp} (μm)
Jaouen *et al.*[14]	0.005	0.02		
Rho *et al.*[16]	0.5	2.05	0.1	0.41
Um *et al.*[11]	2	8.20	2	8.20
Parthasarathy *et al.*[17]	0.0074	0.03		
Parthasarathy[a] *et al.*[18]	0.087	0.36		
Beattie[b] *et al.*[19]	0.13	0.53		

[a] T = 80°C.
[b] T = 70°C.

Acknowledgments

The authors thank Michael Löhr for the conduction of experiments and Peter Berg, Brian Wetton, and Keith Promislow for their helpful comments. A.G. gratefully acknowledges funding by Ballard Power Systems, Inc. and The Mathematics of Information Technology and Complex Systems.

Ballard Power Systems, Incorporated assisted in meeting the publication costs of this article.

Appendix

In this appendix we describe the solution of Eq. 6-10. z is the axis across the GDL perpendicular to the membrane, $z \in [0,L]$, where L is the width of the GDL. The interface between the catalyst and GDL is located at $z = 0$ and at $z = L$ is located the interface between the channel and the GDL. $c(z,t)$ and $c_{ch}(t)$ denote the concentration of O_2 in the GDL and flow channel, respectively.

Nondimensional formulation.—It is convenient to introduce the nondimensional variables $\tilde{z} = z/L$, $\tilde{t} = t \cdot D/L^2$. Equations 6-10 become

$$\frac{\partial}{\partial \tilde{t}} c(\tilde{z},\tilde{t}) = \frac{\partial^2}{\partial^2 \tilde{z}} c(\tilde{z},\tilde{t}) \qquad [A\text{–}1]$$

$$c(\tilde{z},0) = c_0 \qquad [A\text{–}2]$$

$$\frac{4FD}{L} \cdot \frac{\partial}{\partial \tilde{z}} c(0,\tilde{t}) = i \qquad [A\text{–}3]$$

$$c(1,t) = c_{ch}(t) \qquad [A\text{–}4]$$

where the equations for $c_{ch}(t)$ are

$$\begin{cases} \dfrac{\partial}{\partial \tilde{t}} c_{ch}(\tilde{t}) = \dfrac{-LA}{V_{ch}} \cdot \dfrac{\partial}{\partial \tilde{z}} c(1,\tilde{t}) \\ c_{ch}(0) = c_0 \end{cases} \qquad [A\text{–}5]$$

In what follows, we write z,t instead of $\tilde{z},\tilde{t}$.

Discretization.—As all the oxygen initially present in the flow channel becomes consumed, the concentration vanishes at a finite time, say τ. We take small time intervals $[t_l,t_{l+1})$, $l \geqslant 1$ with $t_1 = 0$ and constant increments $t_{l+1} - t_l = \Delta t$, which we take as small as 5×10^{-4} s to make sure the results are accurate within 5%.

The process to solve for $c(z,t)$ is iterative in l, the time-step interval. For each l, the solution $c^l(z,t)$ involves an infinite sum in cosines; for our accuracy purposes of 5%, it is enough to take the first 100 components (see Eq. A-14).

In each interval, the concentration of oxygen in the channel, $c_{ch}(t)$, is assumed to be constant. After obtaining a solution $c^l(z,t)$ for $z \in [0,1]$ and $t \in [t_l,t_{l+1})$, at $t = t_{l+1}$, the concentration is updated using Eq. A-5. Taking the limit $\Delta t \to 0$, keeping τ fixed, provides the analytic solution $c(z,t)$ (see Fig. 3).

Discretizing equations A-1-A-5

$$\frac{\partial}{\partial t} c^l(z,t) = \frac{\partial^2}{\partial^2 z} c^l(z,t) \quad z \text{ in } [0,1],\ t \in [t_l,t_{l+1}) \qquad [A\text{–}6]$$

$$c^l(z,t_l) = c^{l-1}(z,t_l) \qquad [A\text{–}7]$$

$$\frac{\partial}{\partial z} c^l(0,t) = a \qquad [A\text{–}8]$$

$$c^l(1,t) = e_l \qquad [A–9]$$

where the value for $c^{l-1}(z,t)$ is calculated from the previous step, with $c^0(z,t_1) = c_0$, $a = iL/4FD$, and $e_l = c_{ch}(t_l) = e_{l-1} + \Delta t(-AL/V_{ch}) \cdot \partial/\partial z c^{l-1}(1,t_l)$, for $l \geqslant 2$, with $e_0 = e_1 = c_0$. Equation A-7 is a continuity condition: the initial value for c^l, at $t = t_l$, is given by c^{l-1} at the end of its time interval.

We set the boundary conditions at $z = 0$ and $z = 1$ according to the change of variables

$$c^l(z,t) = W^l(z,t) + a \cdot z + e_l - a$$

and solve

$$\frac{\partial}{\partial t}W^l(z,t) = \frac{\partial^2}{\partial^2 z}W^l(z,t) \qquad [A–10]$$

$$\frac{\partial}{\partial z}W^l(0,t) = W^l(1,t) = 0 \qquad [A–11]$$

$$W^l(z,t_l) = W^{l-1}(z,t_l) - (e_l - e_{l-1}) \qquad [A–12]$$

In particular, $W^1(z,0) = b - a\cdot z - e_1 + a$.

By separation of variables, set $W(z,t) = Z(z)\cdot T(t)$, and use Eq. A-10 to obtain $Z(z)\cdot T'(t) = T(t)\cdot Z''(z)$, thus

$$\frac{Z''(z)}{Z(z)} = \frac{T'(t)}{T(t)} =: -\lambda^2$$

so $Z(z) = A\cos(\lambda z) + B\sin(\lambda z)$, $T(t) = \exp(-\lambda^2 t)$, and the general solution to Eq. A-10 is

$$W^l(z,t) = \sum_{n=0}^{\infty}(A_n^l\cos(\lambda_n^l z) + B_n^l\sin(\lambda_n^l z))\exp(-(\lambda_n^l)^2 t)$$

For our accuracy purposes, it suffices to take the first 100 components. For each l, the boundary condition Eq. A-11 gives first $B_n^l = 0$ for all n, and then $\cos(\lambda_n^l) = 0$, or

$$\lambda_n^l = \lambda_n = (2n+1)\frac{\pi}{2} \qquad [A–13]$$

(that is, λ_n^l does not depend on l, the time interval). $\{A_n^l\}_{n=0}^{99}$ can be calculated from Eq. A-12

$$W^l(z,t_l) = \sum_{n=0}^{99}A_n^l\cos(\lambda_n z) = W^{l-1}(z,t_l) - (e_l - e_{l-1})$$

by multiplying both sides by $\cos(\lambda_m z)$ and integrating between 0 and 1; using the orthogonality of the vectors $\{\cos(\lambda_m z)\}_{m=1}^{\infty}$, all these integrals are zero except when $n = m$, in which case

$$\frac{A_n^l}{2} = \int_0^1 (W^{l-1}(z,t_l) - (e_l - e_{l-1}))\cos(\lambda_n z)dz$$

The values for $\{A_n^l\}_{n=0}^{99}$ are then calculated by iteration on l.

Iteration.—We proceed as follows: for $l = 1$ we obtain $\{A_n^l\}_{n=0}^{99}$ as

$$\frac{A_n^1}{2} = \int_0^1 (b - az - e_1 + a)\cdot\cos(\lambda_n z)dz = (b - e_1)\frac{(-1)^n}{\lambda_n} + a\lambda_n$$

where λ_n is as in Eq. A-13. Thus

$$c^1(z,t) = \sum_{n=0}^{99}A_n^1\cos(\lambda_n z)\exp(-\lambda_n^2 t) + e_1 - a + az$$

Assume $\{A_n^{l-1}\}_{n=0}^{99}$ is known. Then

$$\frac{A_n^l}{2} = \int_0^1 (W^{l-1}(z,t_l) - (e_l - e_{l-1}))\cos(\lambda_n z)dz$$

$$= \int_0^1 \left(\sum_{m=1}^{99}A_m^{l-1}\cos(\lambda_m z)\exp(-\lambda_m^2(t_l - t_{l-1}))\right)\cos(\lambda_n z)dz$$

$$- \int_0^1 (e_l - e_{l-1})\cos(\lambda_n z)dz$$

Using the orthogonality of the vectors $\{\cos(\lambda_m z)\}_{m=1}^{\infty}$, the first integral is zero except when $n = m$, therefore

$$\frac{A_n^l}{2} = \int_0^1 \frac{1}{2}A_n^{l-1}\exp(\lambda_n^2(t_l - t_{l-1}))dz - \int_0^1 (e_l - e_{l-1})\cos(\lambda_n z)dz$$

$$= \frac{1}{2}A_n^{l-1}\exp(\lambda_n^2(t_l - t_{l-1})) - (e_l - e_{l-1})\frac{(-1)^n}{\lambda_n}$$

Thus

$$C^l(z,t) = \sum_{n=0}^{99}A_n^l\cos(\lambda_n z)\exp(-\lambda_n^2(t - t_l)) + e_l - a + az$$

The error made in the Fourier series for $c^l(z,t)$ when taking only 100 components, E^l, can be estimated by

$$E^l \leqslant E^1 + 2S(E^1 - a)(2S+1)^l \qquad [A–14]$$

where

$$S = \sum_{n=100}^{\infty}\frac{1}{\lambda_n\exp(\lambda_n^2\varepsilon)} \leqslant \sum_{m=315}^{\infty}\frac{1}{m\exp(m^2\varepsilon)} \leqslant 4\times 10^{-22}$$

$$E^1 = 2\times 10^{-5}\cdot\sum_{n=100}^{\infty}\frac{\lambda_n}{\exp(\lambda_n^2\varepsilon)} \leqslant 2\times 10^{-5}\sum_{m=315}^{\infty}\frac{m}{\exp(m^2\varepsilon)} \leqslant 10^{-21}$$

Thus, for $D = 6.1\times 10^{-7}$ m^2/s, a time-step interval of $\Delta t = 5\times 10^{-4}$, and a channel O_2 consumption time of 5 s

$$E^l \leqslant E^1 + 2S(E^1 - a)(2S+1)^l \leqslant 10^{-21} + 10^{-23}\exp(l2R) \leqslant 10^{-20}$$

List of Symbols

A	cell active area, m^2
A_n^l	nth Fourier coefficient for $c^l(z,t)$, mol/m^3
$b = 2.303\Re T/\alpha nF$	Tafel slope, V
c_{H^+}	proton activity at the catalyst, mol/m^3
c_{H_2O}	water activity at the catalyst, mol/m^3
$c(z,t)$	oxygen concentration in the GDL, mol/m^3
$c(0,t)$	oxygen concentration at the catalyst layer, mol/m^3
$c_{ch}(t)$	oxygen concentration in the channel, mol/m^3
$c_0 = c_{ch}(0)$	initial oxygen concentration, mol/m^3
$c^l(z,t)$	concentration of O_2 in the GDL for $t \in [t_l,t_{l+1})$ (see Appendix), mol/m^3
$D = D_{eff}$	effective diffusion coefficient, m^2/s
$D_{i,j}$	binary diffusion coefficient, m^2/s
D_{O_2}	free space O_2 diffusion coefficient, m^2/s
$E_0 = E_{cell}^0 + \log(i_0)$	fit parameter, V
E, $E_{cell}(t)$	cell voltage, V
$E_{cell}^0(t)$	reversible cell voltage, V
$E_c^0(t)$	reversible cathode potential, V
e^l	value of the concentration of O_2 at the channel for $t \in [t_l,t_{l+1})$, mol/m^3
F	Faraday's constant, 9.648×10^4 C/mol
i	current density, A/m^2
$i_0(t)$	exchange current density, A/m^2
L	thickness of the GDL, m
Q	cell capacity, C
R	cell resistance, Ω m^2
$\Re$	ideal gas constant, 8.314 J/K mol
T	temperature, K
V_{tot}	total cathode free volume, m^3
V_{ch}	channel free volume, m^3

Greek

ε	porosity
$\eta(t)$	overpotential, V
λ_n	nth eigenvalue, m^{-1}

Subscripts

a	anode
c	cathode

References

1. A. Weber, R. Darling, J. Meyers, and J. Newman, in *Handbook of Fuel Cells, Vol. 1*, W. Vielstich, A. Lamm, and H. Gasteiger, Editors, p. 47, Wiley, Chichester (2003).
2. S. Srinivasan, E. A. Ticianelli, C. R. Derouin, and A. Redondo, *J. Power Sources*,

22, 359 (1988).
3. R. Mosdale and S. Srinivasan, *Electrochim. Acta*, **40**, 413 (1995).
4. Y. W. Rho, O. A. Velev, and S. Srinivasan, *J. Electrochem. Soc.*, **141**, 2084 (1994).
5. J. Kim, S. M. Lee, S. Srinivasan, and C. E. Chamberlin, *J. Electrochem. Soc.*, **142**, 2670 (1995).
6. M. Eisenberg, *Electrochim. Acta*, **6**, 93 (1962).
7. G. Squadrito, G. Maggio, E. Passalacqua, F. Lufrano, and A. Patti, *J. Appl. Electrochem.*, **29**, 1449 (1999).
8. A. J. Bard and L. R. Faulkner, *Electrochemical Methods*, p. 250, Wiley, New York (1980).
9. K. Promislow and J. M. Stockie, *SIAM J. Appl. Math.*, **62**, 180 (2001).
10. P. Berg, K. Promislow, J. St. Pierre, J. Stumper, and B. Wetton, *J. Electrochem. Soc.*, **151**, A341 (2004).
11. S. Um, C.-Y. Wang, and K. S. Chen, *J. Electrochem. Soc.*, **147**, 4485 (2000).
12. U. Pasaogullari and C. Y. Wang, *J. Electrochem. Soc.*, **151**, A399 (2004).
13. S. A. Campbell, J. Stumper, D. P. Wilkinson, and M. T. Davis, U.S. Pat. 6,060,190 (2000).
14. F. Jaouen, G. Lindbergh, and G. Sundholm, *J. Electrochem. Soc.*, **149**, A437 (2002).
15. R. H. Perry, *Perry's Chemical Engineer's Handbook*, McGraw-Hill, New York (1984).
16. Y. W. Rho, S. Srinivasan, and Y. T. Ko, *J. Electrochem. Soc.*, **141**, 2089 (1994).
17. A. Parthasarathy, C. R. Martin, and S. Srinivasan, *J. Electrochem. Soc.*, **138**, 916 (1991).
18. A. Parthasarathy, S. Srinivasan, and A. J. Appleby, *J. Electrochem. Soc.*, **139**, 2531 (1992).
19. P. D. Beattie, V. I. Basura, and S. Holdcroft, *J. Electroanal. Chem.*, **468**, 180 (1999).
20. E. A. Mason and A. P. Malinauskas, *Gas Transport in Porous Media: The Dusty Gas Model*, Elsevier, New York (1983).